Evaluating the Theoretical Optical Performances of Colloidal Quantum Dot Thin Films for Infrared Imaging

Arthur Arnaud[1], Bilal Chehaibou[1,2,3], Gabriel Mugny[4], L Baudoin[1], P Machut[3,4], B Rae[5], A G Pattantyus-Abraham[6], Jonathan Steckel[4], Peter Reiss[3], Christophe Delerue[2]

[1] *STMicroelectronics, Digital FMT, Technology for Optical Sensors, Crolles, France*
[2] *Univ. Lille, CNRS, Centrale Lille, Univ. Polytechnique Hauts-de-France, Junia, UMR 8520 - IEMN, F-59000 Lille, France*
[3] *Univ. Grenoble Alpes, CEA, CNRS, IRIG-SyMMES, STEP, 38000 Grenoble, France*
[4] *STMicroelectronics, Analog, MEMS & Sensors Group, Imaging, Grenoble*
[5] *STMicroelectronics Analog, MEMS & Sensors Group, Imaging, Edimburgh, Scotland, UK*
[6] STMicroelectronics, Digital FMT, Technology for Optical Sensors, Fremont/Santa Clara, CA, USA

Abstract— **Research on the development of thin films made of colloidal Quantum Dots (CQDs) has progressively gained interest due to their optoelectronic properties and potential low-cost manufacturing. The ability to tune the first absorption feature of CQDs by changing their material composition, particle size and shape, and/or the surrounding dielectric environment (ligands) is particularly interesting for improving the performance of image sensors in the Near-Infrared (NIR) and Short-Wave Infrared domain (SWIR) where silicon poorly absorbs photons or has no absorption at all. To date, few papers have attempted to evaluate the best optical performances that can be achieved with CQD thin films. In this work, we present the results from our compact model mixing tight-binding simulations, effective medium theory and optical simulations, to explain the various factors impacting CQD photodiode performance and to compare their performance with classical bulk semiconductors like silicon, germanium and III-V's.**

Keywords—Colloidal quantum dots, Image sensors, SWIR, NIR, tight-binding, effective medium theory

I. Introduction

Since pioneering works by Ekimov, Efros and Brus in the 1980s [1], research on colloidal quantum dots (CQDs) has rapidly progressed, moving from academic research to the display industry and now to the microelectronics industry. Their excellent optical properties due to their exciton quantum confinement capability, as well as the low production costs related to their chemical synthesis and the easy large-scale integration into standard microelectronic flows have already allowed the development and commercialization of TV displays, and lighting solutions. Their ability to operate in ranges covering the ultraviolet, visible, and infrared, leveraging electrically passive optical-optical transduction, where the absorption of photons by CQDs are re-emitted at precisely engineered wavelengths determined by the size of the nanocrystals and the material from which they are made is very unique [2].

The use of CQDs for image sensors or photovoltaic cells is more complex because it requires the development of thin layers of nanocrystals with high optical absorption coefficients and good electronic properties to allow the transport of photogenerated charges towards the collecting electrodes [3,4]. The use of photodiodes based on CQDs is unlikely to compete with the use of silicon as a photodetector in the visible range, but it is very promising in the regions of the optical spectrum where silicon is less sensitive, especially in the NIR and SWIR portion of the spectrum where silicon becomes almost transparent. For these parts of the light spectrum, the most used bulk semiconductors are III-V materials such as InGaAs which can provide quantum efficiencies close to 100% with epitaxies of about 2 micrometers thickness. However, the use of an InGaAs photodiode to make image sensors is both complicated and expensive, due to the use of InP wafers for the realization of InGaAs epitaxy, but also due to the need for die-to-die or die-to-wafer hybridization to make functional image sensors. The resulting prohibitive costs (>1000$ per unit) currently limit their deployment for consumer applications. For infrared imaging applications, the use of CQDs is particularly attractive to reduce the cost of the sensors to a few dollars per unit thanks to their easy integration. At the same time, QD technology is also particularly suitable for applications requiring active light systems like Direct and Indirect Time-of-Flight (ITOF, DTOF) and structured light applications, where the presence of sharp excitonic peak due to the first $1s_e$-$1s_h$ transition allows improving the rejection rate of the solar background at the solar spectrum local minima, around the 940 nm, 1130 nm, and 1360 nm wavelengths.

To improve the performance of image sensors using CQD thin films as absorbers, it is necessary to understand and model accurately their optical properties and to understand the role of the nanoparticles and the ligands used to passivate the interface states on the surface of the nanoparticles. In this paper, after a brief presentation of the architecture of CQDs image sensors, we will present a complete physical model using Empirical Tight-Binding Method (ETBM) to evaluate the intrinsic optical properties of the nanoparticles, the Effective Medium Theory to calculate the optical indices of the thin films, and the transfer matrix method to optimize the performance of the photodiodes integrating these same thin films within a resonant cavity. Thus, we will be able to compare the maximum theoretical optical performances of CQDs made of different semiconductor materials with other bulk semiconductors such as InGaAs, germanium, silicon and silicon-germanium, and to show the interest in using quantum confinement to boost the sensitivity of image sensors for infrared sensing applications.

II. Colloidal quantum dots diode model

A. *Generic structures of CQDs photodiodes*

Although the CQD-based image sensors presented in the literature [5-8] can diverge in terms of design options for the photodiode signal readout, or on the choice of the CQD materials (PbS, HgTe, InAs...), most of them are based on the integration of a vertical CQD photodiode built above the Back-end-of-Line (BEOL), with the collection of the photogenerated charges on the photodiode bottom electrode (Fig.1). The integration of the active layer of passivated QDs is generally performed by full-wafer spin-coating of the colloidal QDs, with a replacement of the long-chain ligands by short-chain ones, realized either before deposition in solution (solution ligand exchange) [9], or directly on the wafer (solid-phase ligand exchange, which may require a layer-by-layer process) [10]. The realization of a photosensitive layer continuous over the full pixel matrix and above the metal interconnections has two advantages beyond its simple realization: it allows to obtain pixels with a 100% fill factor, but also the reduction of the pixel pitch, as the photodiode is no longer integrated at the silicon surface as the transistors of the pixel. With this approach, we have demonstrated the operation of a global shutter pixel with a pitch of 1.62um with 50% of EQE at 940 nm and 60% of EQE at 1400 nm [5].

Even if ligands are not directly involved in the film's light absorption (though they modulate the properties of the film as we will

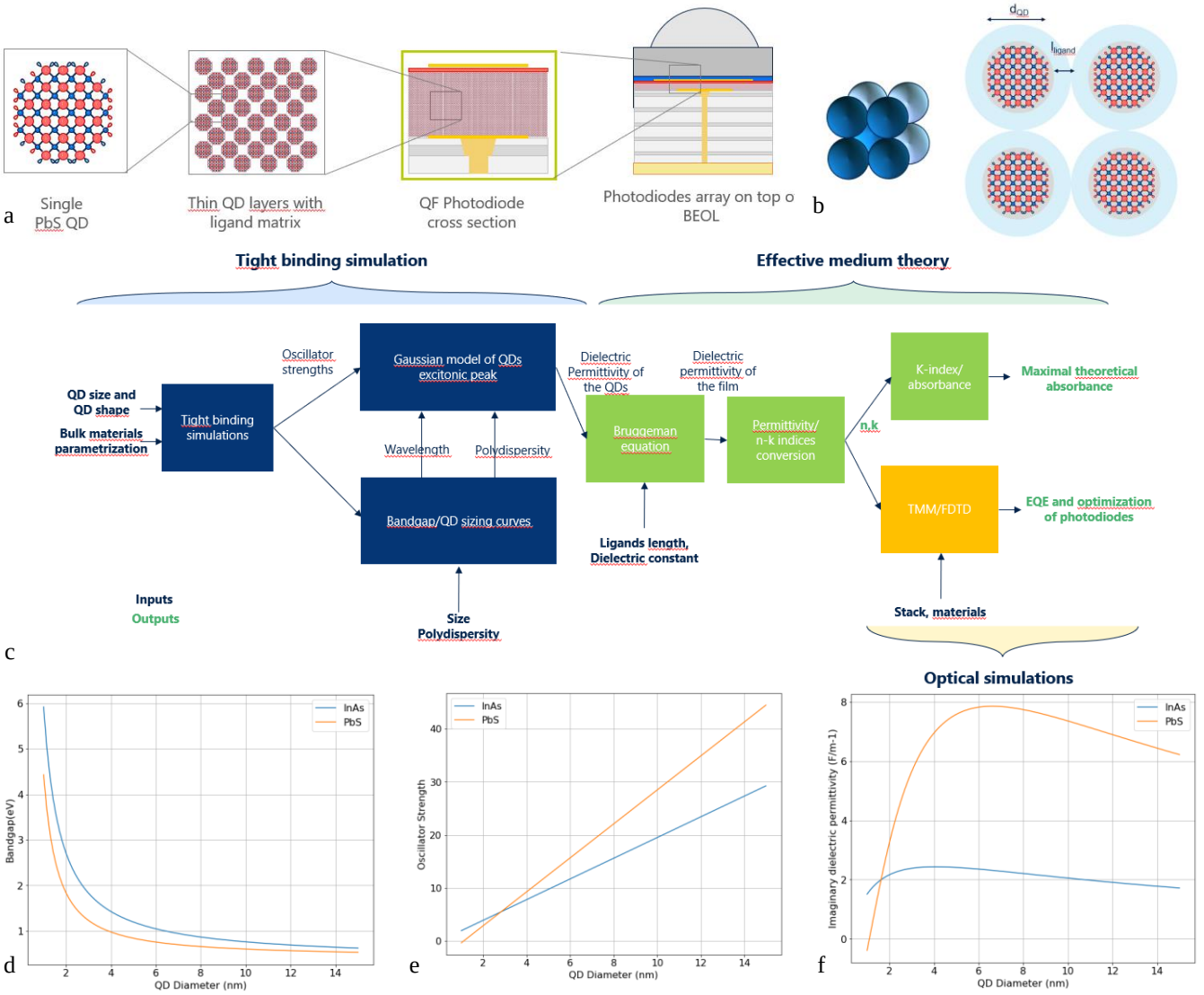

Figure 1. a. Generic scheme of the integration of a CQD photodiode above BEOL. b. Simplified scheme of close-packed passivated QDs inside thin films. c. Diagram representing the compact model stages. d. Polynomial fit of the optical bandgap of QDs vs QD diameter for PbS and InAs. e. Linear fit of the oscillator strength for PbS and InAs QDs. f. Extraction of the imaginary dielectric parts for PbS and InAs QDs.

show here), their choice is important for the operation of the photodiode. Passivation of the interface states by the ligands primarily reduces trapping and recombination phenomena in the film, improving the dark current of the photodiode. The use of short-chain ligands to passivate CQDs is also required to increase the density of QDs in the film but also to improve the electrical transport properties of the film, as the photogenerated charges pass from one QD to the other through a mechanism of variable-range hopping [11]. The ligands having a non-zero net charge, they also participate in the effective film doping [12] and also modify the workfunction of the QD layer through their dipole moment creating a local electric field around the QDs [13]. This last property enables the creation of heterojunctions by using different types of ligands within the same photodiode. Finally, they contribute to the mechanical and chemical stability of the thin films.

In this paper, we will only focus on the optical properties of CQD thin films. To understand the impact of the QDs and ligands properties on the photodiode performances, we developed a multiscale compact model represented in Fig.1c, based on the combined use of ETBM [14] to simulate the dielectric properties of isolated QDs, of the Bruggeman equation to describe the properties of CQD thin films, and finally of the Transfer Matrix Method to compute the performance of vertical photodiode stacks. The QDs' physical parameters taken into account are their size and shape, the properties of the semiconductor they are made of, and the size polydispersity, a parameter controlled during their chemical synthesis. In the case of ligands, we only consider their effective length and their optical indices.

B. Intrinsic properties of QDs

First, the electronic structure of the nanocrystals was calculated using the TB_Sim software [14] to describe the evolution of the optical bandgap and the oscillator forces of the QDs as a function of the size of the QDs, their geometry and the semiconductor material from which they are made. The interest of ETBM over Density Functional Theory (DFT) method is to quickly calculate the oscillator strengths for QDs of several nanometers without being limited by the computational resources. The compilation of these two data, oscillator forces and optical bandgap, allows us to extract the coefficients specific to the QD materials, to approximate optical bandgap variations with $1/d_{QD}$ polynomials (Fig.1d) and oscillator strength with linear regression as explained in [14] (Fig.1e). Finally, we use the two latter quantities along with the size polydispersity to input an analytical equation of the imaginary part of the dielectric permittivity Im[ε] [14]. It allows us to evaluate Im[ε] at the first exitonic peak for a broad range of QD sizes as shown in Fig 1.f for lead sulfide and indium arsenide QDs.

III. Performance of CQD thin films

A. *CQD thin film dielectric model*

Once the properties of the isolated QDs have been modeled, it is necessary to understand the dielectric interactions between the QDs and the ligands and how they affect the optical properties of the thin films. To do so, we must first make simplifying assumptions on the arrangement of the QDs within the thin films by considering that the QDs passivated by the ligands tend to be organized in a body-centered cubic superlattice within the thin films [15]. The fact that ligands are short, and the results presented in [17] allow us to assume that each passivated QD behaves as a rigid sphere. It is then possible to define the packing of the nanocrystals superlattice and to calculate the QDs' density within the film as a function of the QD diameter and the ligand length. This calculation is mandatory for the implementation of Bruggeman's effective medium approximation which accurately describes the dielectric behavior of CQDs thin films [16,17], by using the n and k indices of the QDs. These are derived from the QDs' dielectric constant imaginary part, the bulk semiconductor dielectric constant real part and the refraction index of the ligands as extracted in [17] (ligands do not contribute to the absorption (k_{ligand}=0)).

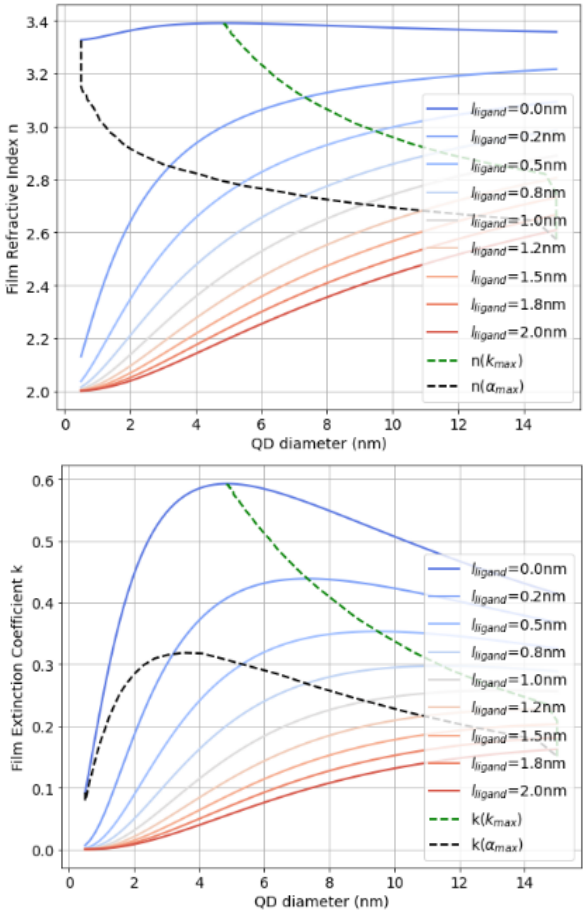

Figure 2. Evolution of the refractive index (a) and extinction coefficient k (b) of PbS QDs with 4% size polydispersity for several ligand length values.

B. *Influence of ligand length*

Figure 2 illustrates the dependence of n and k indices of thin films on QD's diameter for various ligands length assuming a size polydispersity of 4%. These curves first demonstrate the interest in reducing the inter-QD distance to densify CQDs thin films to finally increase the probability for a QD to capture a photon. The second interesting observation is the existence of an optimal QD size for each fixed ligand length that maximizes the extinction coefficient k or the absorption coefficient (not represented here) whose loci are represented by a dashed curve in Fig.2. The existence of this optimum can be explained by the fact that whereas decreasing the QD size helps to enhance the quantum confinement and extinction coefficient of individual QDs first, below a given diameter, the reduction of QDs' size strongly impacts the QDs volume fraction in the film, counterbalancing the confinement effect, hence leading to a reduction of the absorption coefficient of the thin film.

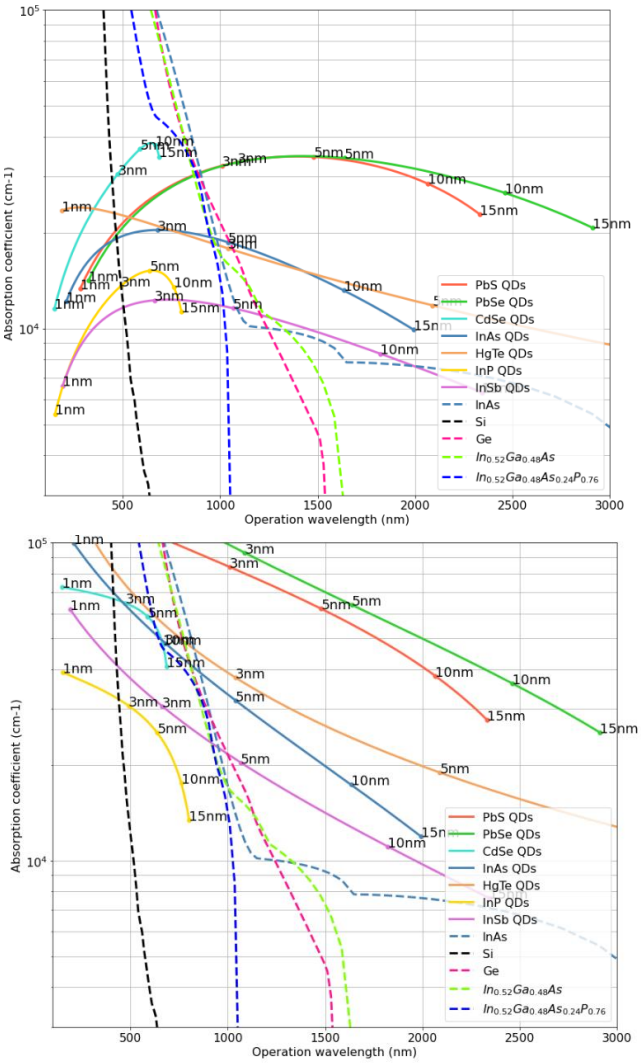

Figure 3. a. Evolution of the absorption coefficient of QDs at the excitonic peak wavelength for a ligand length of 0.4 nm and a size dispersity of 4%. b. Optical performances assuming the formation of superlattices of connected quantum dots.

C. *Comparing quantum dots materials with other semiconductors*

The previous study performed on lead sulfide QDs has been systematically performed on other semiconductor materials: PbSe, CdSe, InP, InAs, InSb, and HgTe. Fig. 3 compiles the absorption coefficients for all these materials as a function of the wavelength of the first excitonic peak to compare CQDs materials with each other and with other bulk semiconductors, without any reference to QDs' diameters but only to the application wavelength. Fig.3a shows the performances of QDs passivated with 0.4 nm-long ligands and 4% polydispersity while Fig.3b shows the performances of thin films with QDs touching each other [18]. These two graphs demonstrate that it is easily possible to exceed the optical performances of silicon with InAs, InSb, HgTe, PbS and PbSe CQDs in the infrared but also to create highly absorbent thin films performing better than Germanium and III-V for wavelengths above 1.0 µm by improving QDs size polydispersity and inter-QDs distance.

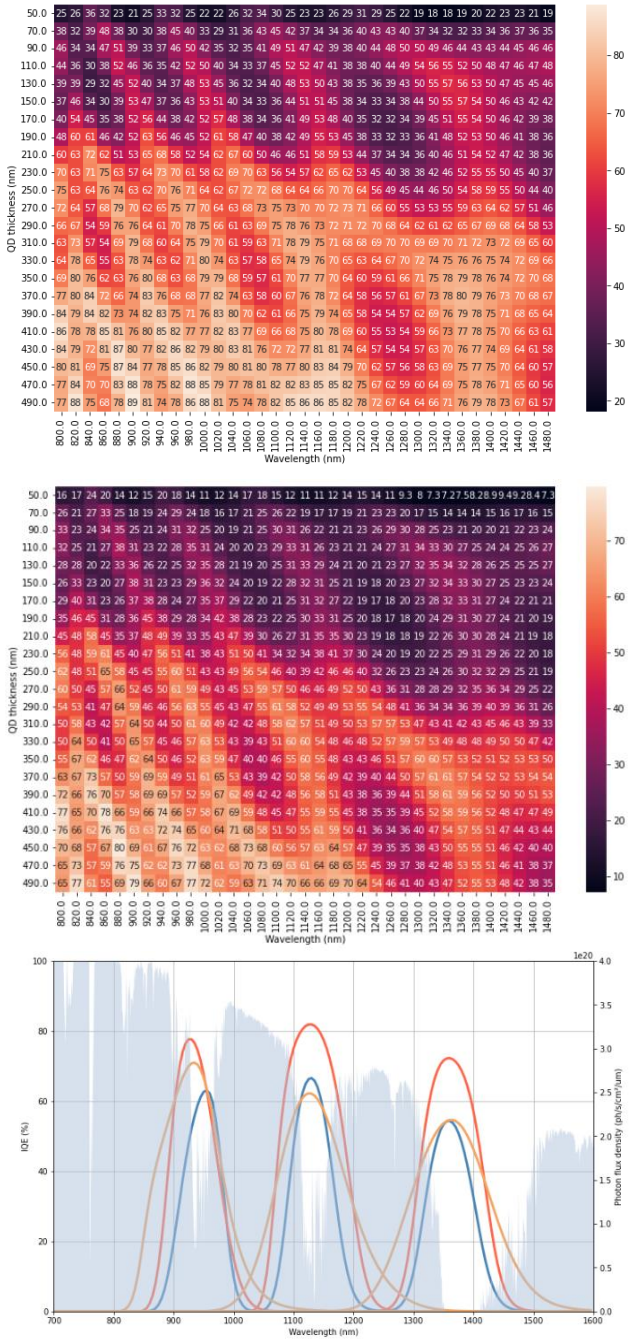

Figure 4. a. EQE maps assuming 4% size dispersion and 0.4 nm-long ligands for PbS (a) and InAs (b). c. Performances of photodiodes at the excitonic peak wavelength, with a QD layer thickness around 300 nm for the same size dispersion and ligand length (red: PbS, orange: InAs, Blue: HgTe). Absorption of QDs at higher energy than excitonic peak is not simulated.

IV. Performances of CQD photodiodes

To illustrate what these different theoretical performances represent in terms of quantum efficiency for photodiodes, we simulated a simple stack of vertical photodiodes using the transfer matrix method and the n and k indexes previously calculated. Figures 4a and 4b show the results of the optimization of the QDs thin film thickness at different wavelengths for PbS and InAs QDs, the QDs' diameter being each time adjusted so that its excitonic peak corresponds to the incident light wavelength. The obtained EQE maps illustrate the need to increase the thickness of the material's layer to improve the photodiode quantum efficiency but also the existence of resonant cavity phenomena, with the presence of local maxima and minima for thin cavity depths.

Finally, we present in Fig.4c the optical performances related to the excitonic peak only for PbS, HgTe and InAs QDs (the other transitions and the high energy absorption not being considered in this reduced model), assuming photodiodes with a 300 nm thick QD layer (polydispersity of 4%, 0.4 nm-long ligands) without anti-reflective coating on top of the photodiodes. This shows that the excitonic peak transition can allow reaching EQE values above 60% at 940 nm with a thin layer of PbS QDs exhibiting a sharp transition and good rejection ratio of solar background for wavelengths above the excitonic peak, and low cross-talk due to the small thickness of the CQD layer. These results illustrate the potential benefits of using CQD photodiodes for active light systems in infrared applications.

V. Conclusion

In this paper, we presented a methodology to simulate the optical properties of QDs thin films and to predict the quantum efficiencies of CQD-based photodiodes using classical optical simulation methods. This study has allowed us to explain the role of different material parameters (QD size, material choice, ligand length, polydispersity, thin film thickness) impacting the performance of thin films. We showed in particular that it is possible to obtain materials with better performances than established III-V technologies by improving the polydispersity and the volume fraction of QDs in thin films, and by favoring materials such as PbS, PbSe, HgTe and InAs for infrared applications. This reduced model thus represents an appealing tool to anticipate technological developments that can be used for standard imaging applications as well as for the development of a model of CQD hyper-spectrometers for example.

References

[1] Efros, A. L.; Brus, L. E. *ACS Nano* **2021**, *15* (4), 6192–6210.
[2] Talapin, D. V.; Steckel, J. *MRS Bulletin* **2013**, *38* (9), 685–691.
[3] Kagan, C. R.; Lifshitz, E.; Sargent, E. H.; Talapin, D. V. *Science* **2016**, *353* (6302).
[4] Carey, G. H.; Abdelhady, A. L.; Ning, Z.; Thon, S. M.; Bakr, O. M.; Sargent, E. H. *Chemical Reviews* **2015**, *115* (23), 12732–12763.
[5] Steckel, J. S. et al *2021 IEEE International Electron Devices Meeting (IEDM)* **2021**.
[6] Georgitzikis, E.; Malinowski, P. E.; Li, Y.; Maes, J.; Hagelsieb, L. M.; Guerrieri, S.; Hens, Z.; Heremans, P.; Cheyns, D. *IEEE Sensors Journal* **2020**, *20* (13), 6841–6848.
[7] Hinds, S.; Klem, E.; Gregory, C.; Hilton, A.; Hames, G.; Violette, K. *Infrared Technology and Applications XLVI* **2020**.
[8] Gréboval, C.; Darson, D.; Parahyba, V.; Alchaar, R.; Abadie, C.; Noguier, V.; Ferré, S.; Izquierdo, E.; Khalili, A.; Prado, Y.; Potet, P.; Lhuillier, E. *Nanoscale* **2022**, *14* (26), 9359–9368.
[9] Nataliia Sukharevska, N.; Bederak, D.; Goossens, M.; Momand, J.; Duim, H.; Dirin, D.;Kovalenko, M.; Kooi, B.; Loi, M.; *ACS Appl. Mater. Interfaces* **2021**, 13 (4), 5195–5207
[10] Luther, J. M.; Law, M.; Song, Q.; Perkins, C. L.; Beard, M. C.; Nozik, A. J. *ACS Nano* **2008**, *2* (2), 271–280.
[11] Guyot-Sionnest, P. *The Journal of Physical Chemistry Letters* **2012**, *3* (9), 1169–1175.
[12] Voznyy, O.; Zhitomirsky, D.; Stadler, P.; Ning, Z.; Hoogland, S.; Sargent, E. H. *ACS Nano* **2012**, *6* (9), 8448–8455.
[13] Brown, P. R.; Kim, D.; Lunt, R. R.; Zhao, N.; Bawendi, M. G.; Grossman, J. C.; Bulović, V. *ACS Nano* **2014**, *8* (6), 5863–5872.
[14] Delerue, C.; Lannoo, M. *Nanostructures: Theory and Modelling*, Springer, **2004**
[15] Weidman, M. C.; Beck, M. E.; Hoffman, R. S.; Prins, F.; Tisdale, W. A. *ACS Nano* **2014**, *8* (6), 6363–6371.
[16] Dement, D. B.; Puri, M.; Ferry, V. E. *The Journal of Physical Chemistry C* **2018**, *122* (37), 21557–21568.
[17] Chehaibou, B.; Izquierdo, E.; Chu, A.; Abadie, C.; Cavallo, M.; Khalili, A.; Dang, T. H.; Gréboval, C.; Xu, X. Z.; Ithurria, S.; Vincent, G.; Gallas, B.; Mugny, G.; Arnaud, A.; Lhuillier, E.; Delerue, C. *Nanoscale* **2022**, *14* (7), 2711–2721.
[18] Baumgardner, W. J.; Whitham, K.; Hanrath, T. *Nano Letters* **2013**, *13* (7), 3225–3231.